International Journal of Solids and Structures 46 (2009) 125–134

Contents lists available at ScienceDirect

International Journal of Solids and Structures

journal homepage: www.elsevier.com/locate/ijsolstr

Patterned bilayer plate microstructures subjected to thermal loading: Deformation and stresses

Yanhang Zhang [a,b,*], Martin L. Dunn [c]

[a] Department of Mechanical Engineering, Boston University, Boston, MA 02215, USA
[b] Department of Biomedical Engineering, Boston University, Boston, MA 02215, USA
[c] Department of Mechanical Engineering, University of Colorado, Boulder, CO 80309, USA

ARTICLE INFO

Article history:
Received 14 May 2008
Received in revised form 11 August 2008
Available online 28 August 2008

Keywords:
Patterned plate microstructures
Micro-electro-mechanical systems (MEMS)
Thermomechanical deformation
Stress
Curvature
Geometric nonlinearity
Generalized plane strain
Finite element method

ABSTRACT

We studied the deformation of a series of gold/polysilicon patterned plate microstructures fabricated by surface micromachining. The patterned plate microstructures were subjected to a uniform temperature change from 100 °C to room temperature that was intended to induce linear and geometrically nonlinear deformation. We used interferometry to measure full-field deformed shapes of the microstructures. From these measurements we determined the spatially-averaged curvature of the deformed microstructures within individual lines and across the entire plate. The deformation response of the patterned plates can be broadly characterized in terms of the average curvature as a function of temperature change and exhibits linear and geometrically nonlinear behavior. We modeled the deformation response of the patterned plates using geometrically nonlinear plate theory with the finite element method. Good agreement was obtained between predictions and measurements for both local curvature variations across lines and for the evolution of curvature of the entire plate with temperature change. Using a generalized plane strain approach with the finite element method we also modeled the spatial dependence of the stress distribution in the lines and substrate. For thick plates, our results agree with those of previous studies, showing a decrease in the von Mises stress in the metal lines with decreasing linewidth. For thinner substrates, though, we find the behavior with linewidth is opposite and there is a critical substrate thickness (about 10 μm for the system in our study) where the behavior with linewidth changes. These results have important implications in the design of patterned structures for micro-electro-mechanical systems (MEMS) applications where films are of comparable thickness to the underlying substrate.

Published by Elsevier Ltd.

1. Introduction

Multilayer film systems find widespread applications in many technological arenas including electronics, optoelectronics, photonics, information storage, displays, solar cells, modern batteries, and a variety of micro and nanosystems. In these arenas, many different film materials, including metals, ceramics, and polymers, are used and they are realized via many fabrication processes that typically include deposition, patterning, and etching (see, for example, Freund and Suresh, 2003). During the multiple thin-film deposition and etching processes, as well as during subsequent post-processing/packaging and use, many complicated mechanisms occur which result in straining of the film layers, and these generally differ from layer to layer. These film strains from various sources including lattice mismatch, microstructural

* Corresponding author.
E-mail address: yanhang@bu.edu (Y. Zhang).

0020-7683/$ - see front matter Published by Elsevier Ltd.
doi:10.1016/j.ijsolstr.2008.08.020

evolution, and thermal expansion mismatch among others. The requirement that the film layers maintain coherency at the interfaces between them means that these strains cannot occur freely, and thus they are constrained, which results in stresses in the layers and curvature of the multilayer film system; both of these can have significant practical implications on device yield and reliability. In many microelectronic or micro-electro-mechanical systems (MEMS), films are nonuniformly patterned onto a substrate or other film layers. A common example consists of metal lines on a substrate that are used to supply power, or as signal input and output, to a device. In systems containing arrays of micromechanical components, the necessary metallization for power and signal lines is typically fabricated in the form of a periodic array. For example, on top of a silicon substrate, multiple films of metal lines encased in a dielectric are deposited. The thermoelastic mismatch between materials due to the metallization can lead to stress and deformation either upon uniform or localized temperature changes. The former can arise as a result of various processes during fabrication, packaging, and use. The latter can result from Joule heating during current flow (Shen, 2001; Kim and Lin, 2005; Keller et al., 2007). Furthermore, film patterns can be designed to yield specific device performance due to the interaction of misfit strains and pattern geometry (Pajot et al., 2006). Finally we note that technological trends are continually resulting in thinner and thinner films which make issues of dimensional stability due to misfit strains increasingly important.

Numerous studies have elucidated the basic thermomechanical response of multilayer material systems when subjected to temperature changes or other sources of misfit strains between the layers. These have come in the context of many technological applications, the most common being structural composite materials (Hyer, 1981, 1982), thin-film/substrate systems for microelectronics (Fahnline et al., 1991; Masters and Salamon, 1993, 1994; Finot and Suresh, 1996; Finot et al., 1997; Freund, 1993, 1996, 2000; Freund and Suresh, 2003), thin-film systems for MEMS (Dunn et al., 2002; Zhang and Dunn, 2003, 2004), and photoactive polymer systems (Dunn, 2007). Due to this voluminous literature on the subject of fully covered film systems, we will not elaborate further on them, but instead focus our remaining introductory comments on patterned film systems.

Motivated by microelectronics applications, curvature and stress development has been studied for substrates covered with films patterned in periodic lines (Yeo et al., 1995a; Yeo et al., 1995b; Park and Suresh, 2000; Gouldstone et al., 1998; Wikstrom et al., 1999a; Wikstrom et al., 1999b; Wikstrom and Gudmundson, 2000; and Shen et al., 1996). Wikstrom et al. (1999a) analyzed the thermoelastic stresses and curvatures arising from patterned thin lines on substrate both analytically and numerically. In the analytical approach, an analogy was made with anisotropic plates with surface cracks to yield an approximate solution for volume-averaged stresses in the lines as well as curvature along and normal to the lines. Shen et al. (1996) modeled the evolution of stresses and curvature due to patterning of silicon oxide lines on silicon wafers. They used a generalized plane strain finite element formulation to compute curvatures along and normal to the lines. They showed, both experimentally and theoretically, reversals of curvature in the direction perpendicular to the lines, and suggested this effect is due to the Poisson effect from the anisotropic strain coupling in the patterned structures. Park and Suresh (2000) presented an analytical model based on a composite analogy. A layer consisting of copper and oxide lines is modeled as a homogenized composite layer and the effective thermoelastic properties of the composite layer are computed using standard composite theory. These studies have shown that patterning in the form of lines can substantially impact the curvature of the thin-film/substrate system and the stress state in the lines both along and across the direction of the lines. In a series of recent papers, Huang, Rosakis, and colleagues have studied a range of film/substrate problems involving nonuniform misfit strain, temperature, and thickness distributions (Park et al., 2003; Ngo et al., 2006, 2007; Brown et al., 2007; Feng et al., 2007a,b). A key result of this body of work was the identification, theoretically and experimentally, of the connection between the nonuniform distribution of stresses in the films and the overall curvature of the film/substrate system. This is technologically significant because the most common experimental technique used to measure film stress in practice is the wafer curvature method where the film/substrate average curvature is measured.

While these studies provide much of the foundational understanding of stresses and deformation of patterned film/substrate systems, especially those with patterned lines, they are not directly applicable to the situation we consider here – a substrate of comparable thickness to the film. We are motivated primarily by MEMS applications where film layer thicknesses are not only small (on the order of micrometers) relative to in-plane dimensions, but they are often comparable. This can lead to much larger deflections, relative to the thickness of structures, than are observed in microelectronics applications, and make it necessary to include geometric nonlinearity in order to accurately model deformation. Furthermore, the geometric nonlinearity can lead to bifurcations in the deformation behavior for plate-like structures that possess high symmetry. In addition, the curvature, and thus stresses, can vary significantly over the in-plane dimensions of the structure (Finot and Suresh, 1996; Finot et al., 1997; Freund et al., 1999; Freund, 2000; Dunn et al., 2002; Zhang and Dunn, 2004).

In this work we study, via measurements and analysis, the deformation behavior of a series of patterned bilayer plate structures. Our structures, consisting of patterned gold/polycrystalline silicon bilayers, are fabricated using a standard surface micromachining process and subjected to uniform temperature changes that generate internal stresses and deformation via thermal expansion mismatch between the gold and polysilicon. We use interferometry to measure deformed shapes of the bilayers as a function of temperature and present results for both local and average curvature variations. We interpret the measurements with the help of complementary finite element analysis of the deformation of the patterned bilayers, as well as analysis of the thermoelastic stress state in the layers.

2. Samples and measurements

We designed a series of square bilayer plate microstructures (300 μm × 300 μm) consisting of periodic gold lines (0.5 μm thick) on a polysilicon (1.5 μm thick) substrate and fabricated them using a surface micromachining process (Carter et al., 2005). A scanning electron micrograph of a typical patterned plate microstructure is shown in Fig. 1(a); the geometrical parameters used subsequently are defined in Fig. 1(b), where the repeating element is shown. For all bilayer plates, the underlying polysilicon film is the same size (300 μm × 300 μm), and the gold film is patterned into lines of length 300 μm and of width w_1 which is varied to include w_1 = 6, 15, 20, 30, and 50 μm. The line fraction is defined as $c = w_1/w_2$, where w_2 is the width of the repeating cell. We varied the width of the repeating cell, w_2, to include different line fractions from 0 to 0.66. In addition, we fabricated plates fully covered with gold (c = 1.0) and without any gold film (c = 0). The idea behind the designs was to yield plates that rest as freely as possible. To this end, the plates were supported on the substrate by a 16 μm diameter polysilicon post located at the center; due to the conformal nature of the film deposition processes, this can be seen as the *dimple* in the center of the plate in Fig. 1(a).

Our goal is to measure the thermoelastic deformation of the patterned bilayers during uniform temperature changes. This is complicated by the fact that upon deposition and release from the substrate, the material microstructure of the gold films is not in equilibrium. Indeed, as a sample is heated significant microstructural evolution can occur in the gold which results in inelastic straining of the gold film and curvature of the bilayer (Zhang and Dunn, 2003). To ensure, as much as possible, that the deformation we measure is simply thermoelastic we heated the samples above 100 °C and held for ≈3.5 min to stabilize the microstructure. The plates were then cooled to room temperature at a rate of 10 °C/min in a custom-built temperature chamber with optical access. At 100 °C and during cooling we measured full-field out-of-plane displacements of the plate microstructures as a function of temperature using scanning white light interferometry (De Groot and Deck, 1995). The resolution of the out-of-plane displacement measurements is at least 5 nm as verified by making measurements on standards, and the resolution of the temperature chamber is about 1 °C (Zhang and Dunn, 2004). We used a 5X Michelson objective to yield a lateral spatial resolution of about 2.7 μm.

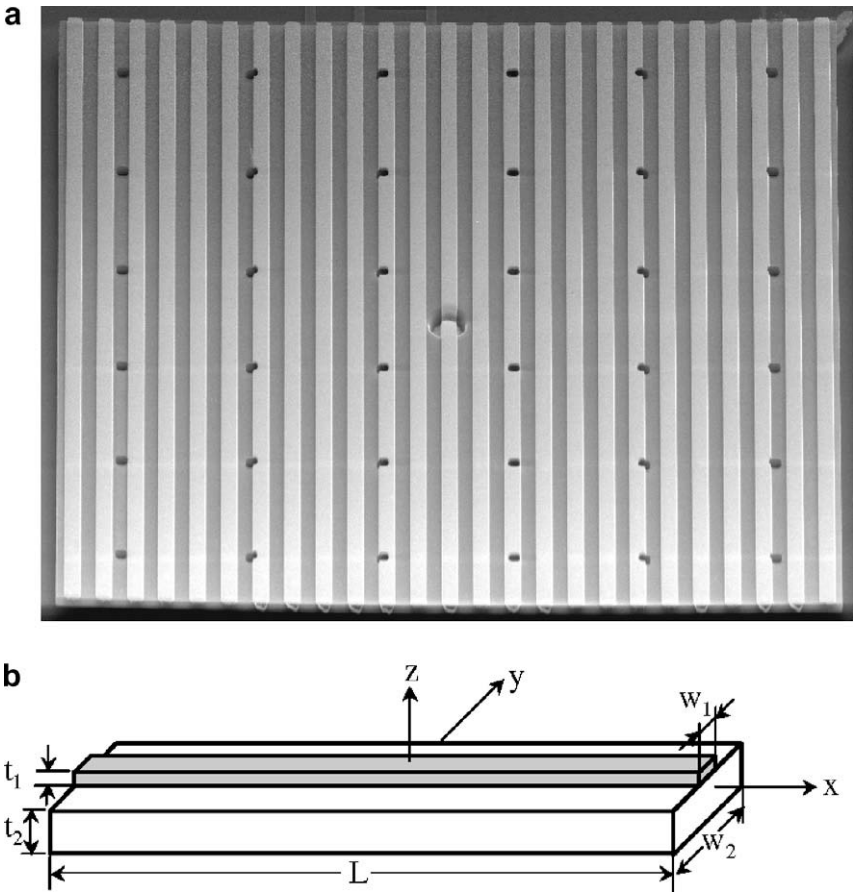

Fig. 1. (a) Scanning electron micrographs of gold (0.5 μm thick)/polysilicon (1.5 μm thick) gold line patterned plate microstructures (300 μm × 300 μm, w_1 = 6 μm, w_2 = 12 μm). (b) Definition of the relevant geometrical parameters for the repeating element; the coordinate system is also shown.

3. Analysis of deformation and stress state

Due to the complexity of the potentially geometrically nonlinear deformation of the patterned plate microstructures, we use the finite element method to model both their overall deformation and the stress state in the lines. Two types of finite element models were used. To model the overall deformation we built a model using four-node composite plate elements to approximate the thin-plate kinematics of the Kirchhoff theory. In this case we modeled the entire square plate and discretized each line individually with finite elements with a characteristic element size of about 1 μm, a size that was chosen after a convergence study with mesh size. To accurately model the stress state in the patterned gold lines, we modeled the repeating element shown in Fig. 1(b) with a generalized plane strain formulation with periodic boundary conditions following Shen et al. (1996), and Ege and Shen (2003). This model assumes straining and bending with constant curvature along the direction of the gold lines, while at the same time accurately describes the spatial dependence of the stress distribution through the cross section of the lines. Typical meshes contain five layers of elements through the thickness of the gold. In both types of finite element models, the constituent materials were assumed to behave elastically, but geometrically nonlinear deformations were allowed.

Input parameters to the finite element calculations are $E_p = 163$ GPa, $\nu_p = 0.22$ (consistent measurements over many MUMPs runs(Sharpe, 2002)), $E_g = 78$ GPa, $\nu_g = 0.42$ (King, 1988). Here and throughout the subscripts p and g denote polysilicon and gold, respectively. The thermal expansion coefficients of polysilicon and gold were assumed to vary linearly with temperature, and values at 100(24) °C are $\alpha_p = 3.1(2.6) \times 10^{-6}/°C$, and $\alpha_g = 14.6(14.2) \times 10^{-6}\ °C^{-1}$ (King, 1988). Consistent with the experiments, calculations were carried out for the loading situation of an applied uniform temperature change from 100 °C to room temperature. In order to understand the effects of the initial curvature at 100 °C on the subsequent nonlinear deformation we carried out two series of calculations with different initial curvatures at 100 °C: (i) the measured curvature and (ii) zero curvature.

4. Results and discussion

4.1. Deformation: local and overall curvatures

Following the basic protocol described in Section 3, we measured the full-field shape of a series of patterned plates as a function of temperature during cooling from 100 °C to room temperature. We also measured uncovered (volume fraction $c = 0$) and fully covered ($c = 1$) plates. During cooling, surface profiles were measured at 10 °C increments; Fig. 2 shows a typical measured surface profile across the lines at the center of a plate. In this case the line width is $w_1 = 30$ μm, $c = 0.5$, and the temperature change is −30 °C; measurements for other samples and temperature changes are similar in character. In Fig. 2, circles represent measurements on the top surface of gold lines and squares represent measurements on the top surface of polysilicon which is not covered by gold. The jump between the circles and squares is due to the thickness of the gold layer and reflects the surface profile of the plate. Fig. 2 shows that at locations where the polysilicon is covered by gold lines, the thermal expansion mismatch between gold and polysilicon cause it to bend upward, however the uncovered polysilicon bends slightly downward. Although not shown, the displacement along the direction of lines varies smoothly on both gold and polysilicon regions. The transverse deformation contours exhibit anisotropy and are elliptical, with the shorter axis aligned with the gold lines.

We determined the average curvature across individual gold lines and polysilicon strips by fitting a polynomial to the measured displacement data and differentiating it twice with respect to position, i.e., $\kappa_x = d^2w/dx^2$ and $\kappa_y = d^2w/dy^2$. We also

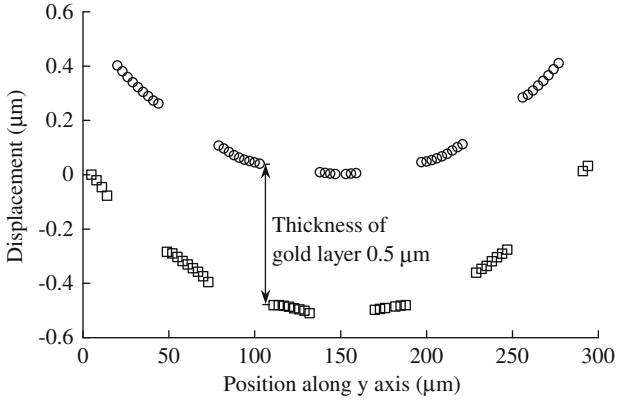

Fig. 2. Surface profile of transverse displacement along $x = 0$ at 70 °C after cooling from 100 °C for a patterned plate microstructure with $w_1 = 30$ μm and $c = 0.5$. Circles represent measurements on the top surface of gold lines and squares represent measurements on the top surface of polysilicon which is not covered by gold.

determined the average curvature over the entire plate in the same manner after subtracting the thickness of the gold film from the measured displacement data. While the curvature perpendicular to the lines was determined from measured displacements across the entire plate, that along the lines was determined over a region of only 150 μm at the center of the plate because the slope of the displacement field outside this region is too large to be measured for the larger temperature changes with the 5X objective.

Fig. 3 shows the measured and predicted average curvature perpendicular to the lines across individual gold lines and polysilicon strips for the sample of Fig. 2. Open symbols are results from predictions and filled symbols are results from measurements. Both measurements and predictions show positive curvature on the gold lines and negative curvature on the polysilicon. We use positive in this study to indicate that the plate bends toward the gold layer. Insufficient displacement data exists to accurately determine the curvature for the polysilicon lines at the edges of the plate. Reasonably good agreement exists between the measurements and predictions. The measured and predicted nonzero curvature in the uncovered region of the multilayer is consistent with recent curvature measurements of tungsten islands on a silicon substrate (Brown et al., 2007), and as they describe, not predicted by the widely-used Stoney equation. The measured curvature over the gold lines, however, increases more than the predictions as the edges of the plate are approached. In our previous studies on fully covered gold/polysilicon structures, the in-plane curvature variation was well captured by similar calculations (Dunn et al., 2002). A possible explanation for the discrepancy here is that the shell elements are not able to fully characterize the details of deformation across the lines, although the average curvature change as a function of temperature can be described reasonably well, as will be shown in Figs. 4 and 5. As we will show in Fig. 6, the stress varies appreciably across the gold lines when the substrate is of comparable thickness to the film, especially for thin lines, and this variation is not well-captured by the shell element model.

In Figs. 4 and 5 we study the effects of line geometry ($c = w_1/w_2$, w_1) on the curvature change as a function of temperature; in Fig. 4 we fix c and vary w_1, while in Fig. 5 we fix w_1 and vary c. Before presenting and discussing these results we comment on a couple of aspects of the measured deformation (curvature) in general. To compare measurements and simulations we use the curvature change during a temperature change. However, negative curvatures are present in the plate structures at 100 °C which is the starting point of the cooling measurements as a result of intrinsic stresses in the films. For $c = 0$, i.e., for bare polysilicon, there is a curvature of about $-75\ \mathrm{m}^{-1}$. This reflects the intrinsic stress gradient in the polysilicon which is 15.7 kPa/μm (Dunn and Cunningham, 2006). As the temperature is decreased the curvature does not change for the bare polysilicon plate. For $c > 0$, i.e., when there are gold lines present, there is a nearly equibiaxial curvature of about $-40\ \mathrm{m}^{-1}$ to $-75\ \mathrm{m}^{-1}$ at 100 °C. This is larger than previous studies with fully covered plates (Zhang and Dunn, 2003, 2004) where the plates were nearly flat. The differences are likely due to intrinsic stress variations between different runs. As the temperature is decreased, the plates start bend upward. The magnitude of the initial curvature is much smaller than the curvature developed during the cooling process, and thus our presentation of the data in terms of curvature change seems reasonable. In the calculations that follow, we consider the significance of the initial curvature on the subsequent nonlinear curvature evolution.

Fig. 4 shows the effect of linewidth on the average curvature development of plate microstructures during the cooling process. Here, the volume fraction is fixed at $c = w_1/w_2 = 0.5$ and the linewidth is varied: $w_1 = 6$, 15, 30, and 50 μm. Open and filled symbols are measurements from two sets of experiments on nominally identical samples, and solid and dashed lines are predictions with and without incorporating the initial curvature at 100 °C. For the same volume fraction of gold coverage, the average curvatures do not vary significantly with linewidth. The curvature along the lines, κ_x, develops almost linearly as a function of temperature change. However, significant nonlinearity exists in the development of curvature perpendicular to the lines, κ_y. κ_y initially increases with temperature change and at about $\Delta T = -20$ °C it starts to exhibit

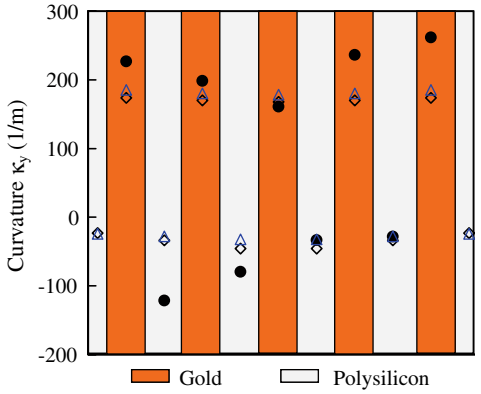

Fig. 3. Average curvature κ_y across individual gold lines and polysilicon areas for the patterned plate microstructure shown in Fig. 2 subjected to a temperature change from 100 to 70 °C. Filled circles are measurements and open symbols are predictions with (open triangles) and without (open diamonds) initial curvature included.

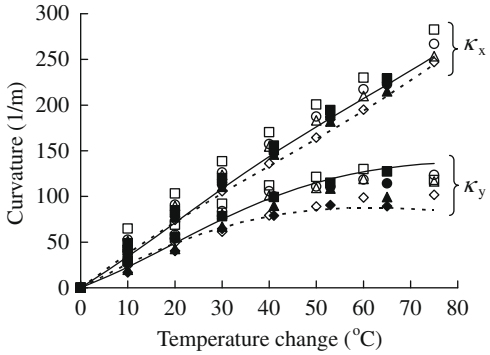

Fig. 4. Average curvature for $c = w_1/w_2 = 0.5$ gold patterned plate microstructures. Open and filled symbols are measurements, and solid and dashed lines are predictions with and without incorporating the initial curvature at 100 °C. Diamonds: $w_1 = 6$ μm; squares: $w_1 = 15$ μm; circles: $w_1 = 30$ μm; triangles: $w_1 = 50$ μm.

nonlinearity. As the temperature change increases κ_y reaches a maximum (at about −65 °C when initial curvature is neglected) and then starts to decrease more slowly as the temperature change increases further. The results from the two experiments show the same behavior and the predictions agree reasonably well with the measurements. When the initial curvature is not considered the predictions are consistently lower than measurements; when the negative initial curvature is incorporated in the calculations the predictions are in better agreement with measurements, although they are actually slightly higher in some cases. The curvature anisotropy that develops immediately upon the temperature change and gradually increases is different than the behavior observed for fully covered plates. There the curvature develops isotropically as the temperature change increases, and depending on the geometrical parameters bifurcates at a critical temperature resulting in curvature anisotropy.

Fig. 5 shows the effect of the volume fraction ($c = 0.3$, 0.5, and 0.7) of patterned gold lines while w_1 is fixed at 30 μm. Open circles are measurements and solid and dashed lines are predictions with and without the initial curvature. For $c = 0.3$ (Fig. 5(a)), κ_x increases almost linearly, while some nonlinearity arises in κ_y as the temperature change exceeds about 30 °C. Both κ_x and κ_y increase as the temperature changes up to 70 °C. For $c = 0.5$ (Fig. 5(b)), κ_x again increases almost linearly, but more significant nonlinearity exists in κ_y. This trend continues for $c = 0.7$ (Fig. 5(c)), where after being linear for about 10 °C, both κ_x and κ_y exhibit nonlinearity, however, the nonlinear behavior of κ_y is much stronger. At about 55 °C, κ_y exhibits a maximum and starts to decrease while κ_x begins to increase at a faster rate. In general, the character of the curvature development with temperature change is similar as the volume fraction increases, but the magnitude of the curvatures and the amount of nonlinearity both increase with increasing volume fraction of gold lines. For all cases, the consideration of the negative initial curvature results in higher predictions that in most cases are in better agreement with measurements. The exception is the transverse curvature κ_y for $c = 0.7$ where predictions are higher than measurements, especially as the temperature change increases.

4.2. Stresses in the patterned lines

Although the finite element models with shell elements reasonably capture the overall curvature development of the patterned plates due to thermal loading, detailed stress distributions in the lines due to edge effect are not accurately modeled. Our calculations with shell elements demonstrate an almost constant stress across the lines and of course do not capture the details of the stress distribution in the load transfer zone near the film edge. Therefore, to better understand the stress state in the patterned lines as a function of temperature change we model the repeating periodic cell using the generalized plane strain formulation, a schematic of the model setup is shown in Fig. 6(a). We modeled the stresses for volume fractions $c = 0.1$, 0.6 and 1, fixing the thickness of the gold at $t_1 = 0.5$ μm and systematically varying the polysilicon thickness from $t_2 = 50$ to 1.5 μm. In these calculations, we ignore any initial curvature; the qualitative results are not affected by the modest negative initial curvatures. In general the stress components vary linearly through the thickness in the gold layers in thin-film systems for MEMS (Zhang and Dunn, 2003). In this study, the stress at the top surface of the gold lines is plotted. Although not shown in the paper, similar trends were found at other locations of the lines.

In Fig. 6, we plot the von Mises stress σ_{vm} at the top surface of the gold lines as t_2 decreases from 50 to 1.5 μm ($t_2 = 50$ μm corresponds approximately to the limit of an infinite substrate). The stress in the film is nearly uniform across the line except for a region of length equal to a few film thicknesses away from the free edge. In this region, shear stresses build up and transfer load between the layers while the normal stress σ_y decreases to zero to satisfy equilibrium. Details of the load transfer mechanism and the nature of the stress state at the free edges of films can be found in Freund and Suresh (2003). The length of this load transfer region does not depend on the linewidth. As a result, if the line is too thin the normal stress never reaches a uniform state. This is apparent as when $t_2 = 50$ μm, σ_{vm} is about the same for $c = 0.6$ and 1, but significantly lower for $c = 0.1$, consistent with the results of studies for patterned lines on thick substrates (Gouldstone et al., 1998; Wikstrom

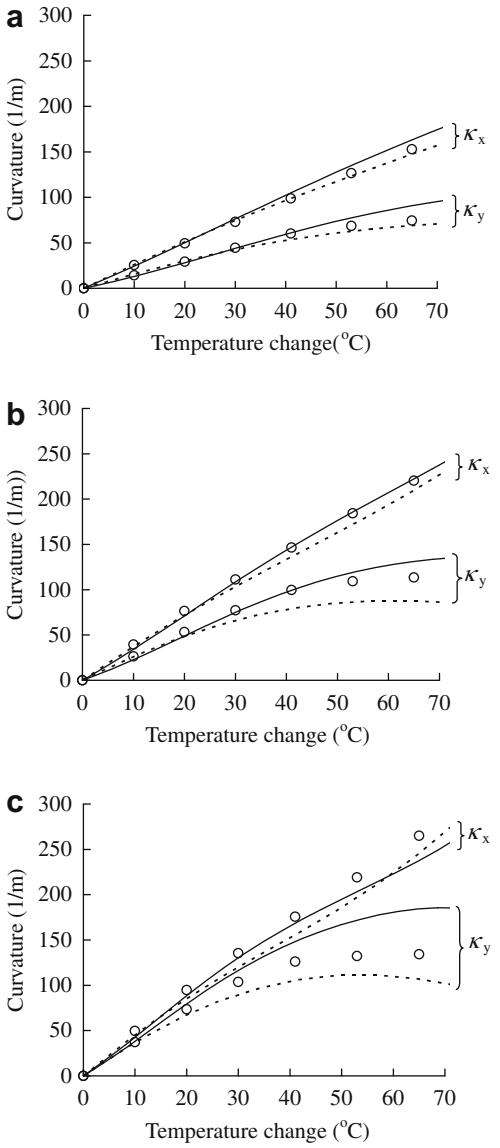

Fig. 5. Average curvature for $c = w_1/w_2$ = (a) 0.3; (b) 0.5; and (c) 0.7 plate microstructures with linewidth w_1 = 30 μm. The curvature along the lines is taken over a 150 μm region at the center, and the curvature across the lines is taken over the whole plate. Open circles are measurements and lines are predictions with (solid) and without (dotted) initial curvature included.

et al., 1999a; Shen et al., 1996). These studies showed that the stress in the lines decreases as the linewidth decreases. Fig. 6 (and Fig. 7) shows that as the polysilicon thickness systematically decreases from the thick substrate limit, σ_{vm} decreases, and the rate of decrease increases dramatically at about t_2 = 10 μm. As a result, when the substrate is thinner than about 10 μm and becomes comparable to the thickness of the gold lines, σ_{vm} is higher in the thinner lines (ignoring the edge effects). This is opposite to the trend predicted for patterned lines on thick substrates (Gouldstone et al., 1998; Wikstrom et al., 1999a; Shen et al., 1996; and some others).

Previously, we showed that upon heating after release inelastic behavior for beams with patterned gold lines commences at about the same temperature independent of linewidth. We suggested that the mechanism responsible for the inelastic behavior is evolution of the nonequilibrium material microstructure and is temperature driven (Zhang and Dunn, 2003). The strong linewidth dependence of stresses shown in Fig. 6 provides further evidence that the inelastic behavior is dominated by temperature instead of stress.

Although not shown here for conciseness, the qualitative behavior of σ_x and σ_y is similar to that of σ_{vm}, although $\sigma_x > \sigma_{vm} > \sigma_y$. A noticeable difference, though, is that the variation of σ_y with linewidth decreases as t_2 decreases; at t_2 = 1.5 μm there is almost no variation of σ_y with linewidth. It is also interesting to mention the combined effect of

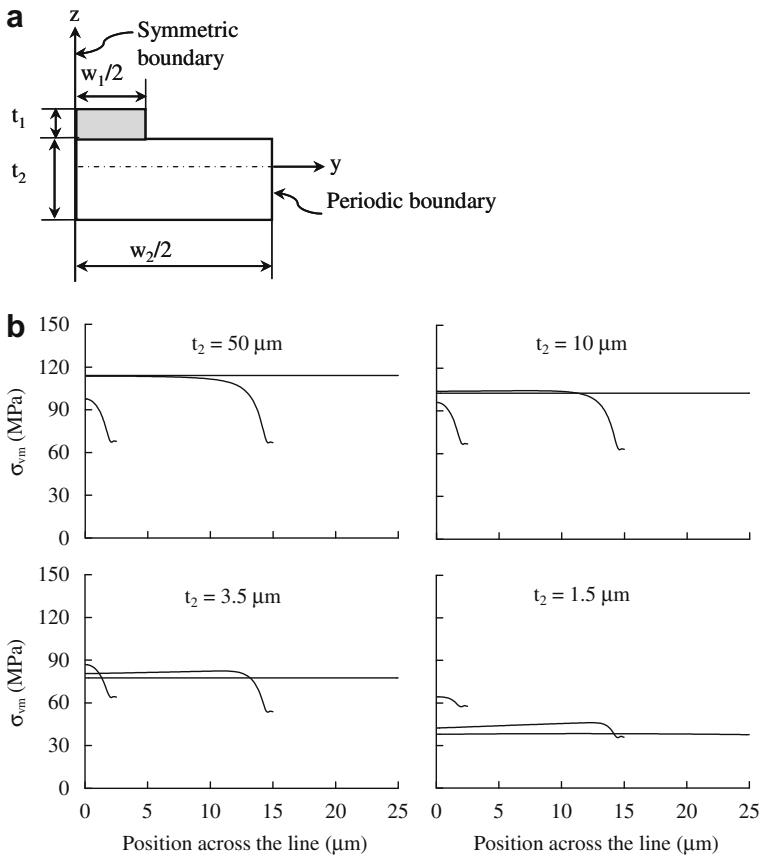

Fig. 6. (a) Schematic of the repeating element of a gold line on polysilicon used for finite element stress calculations; (b) von Mises stress σ_{vm} at the top surface of gold across the line for a gold (0.5 μm thick)/polysilicon (thickness = t_2) periodic cell for $c = w_1/w_2 = 0.1$, 0.6, and 1.

linewidth and substrate thickness on the biaxial stress state in the patterned lines. When the substrate is fully covered, i.e., when $c = 1$, the stress state in the film is equibiaxial so that $\sigma_y = \sigma_x$. When $c = 0.6$, the equibiaxial stress state remains for $t_2 = 50$ and 10 μm, however σ_x is slightly higher than σ_y for $t_2 = 3.5$ and 1.5 μm. When $c = 0.1$, a nonequibiaxial stress state develops in the gold lines for all substrate thicknesses, and is more significant for the lines on thinner substrates. For example σ_x is about twice σ_y for $t_2 = 1.5$ μm. The nonequibiaxial stress state developed is consistent with previous studies of patterned lines on a thick substrate (Gouldstone et al., 1998; Wikstrom et al., 1999a; and Shen et al., 1996).

In Fig. 7, we plot the stress components σ_x, σ_y, and σ_{vm} vs. polysilicon substrate thickness for various linewidths. The stress is taken at the top surface of the gold at the center of the lines. As the polysilicon thickness decreases from the thick substrate limit, the stress in the gold lines/film decreases with a rate that increases strongly as t_2 decreases below about 10 μm. This shows, more clearly than Fig. 6, the behavior of stress in the lines as a function of substrate thickness. For substrates thicker than about 10 μm the stress in the gold is less for thinner substrates while the opposite is the case for substrates thinner than about 10 μm. Previous studies, motivated by microelectronics applications, have been focused on patterned films on thick substrates. The results here are more valuable as guidelines for the design of micro and nanoelectromechanical systems where film layers are often comparable.

5. Summary

We studied the deformation of a series of gold/polysilicon patterned plate microstructures fabricated by surface micromachining and subjected to uniform temperature changes. We used interferometry to measure full-field deformed shapes of the microstructures and from these determined the spatially-averaged curvatured of the deformed microstructures within individual lines and across the entire plate. The deformation response of the patterned plates can be broadly characterized in terms of the average curvature as a function of temperature change and exhibits linear and geometrically nonlinear behavior. Good agreement was obtained between predictions using geometrically nonlinear plate theory and measurements for both local curvature variations across lines and for the evolution of curvature of the entire plate with temperature change. The agreement was better when the negative initial curvature was incorporated into the calculations. For plates with thick substrates relative to the lines, the stress distribution in the lines and substrate, obtained using a

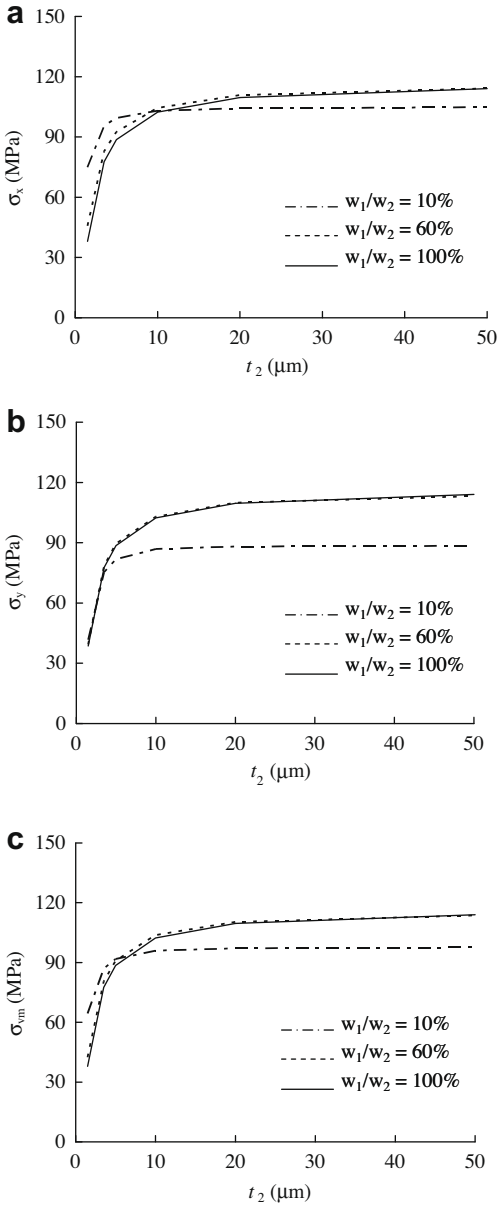

Fig. 7. Stress components at $y = 0$ on the top surface of a line as a function of t_2 for gold (0.5 μm thick)/polysilicon (thickness = t_2) periodic structures for $c = w_1/w_2 = 0.1$, 0.6, and 1: (a) σ_x; (b) σ_y; and (c) von Mises stress σ_{vm}.

generalized plane strain approach, shows a decrease in the von Mises stress in the lines with decreasing linewidth in agreement with previous results. When the substrate becomes comparable to the line thickness we find the behavior with linewidth is the opposite and there is a critical substrate thickness (about 10 μm for the system in our study) where the behavior with linewidth changes.

Acknowledgement

YZ gratefully acknowledges support of the DARPA Young Faculty Award (Award No: W911NF-07-1-0181) and MLD gratefully acknowledges support from the DARPA N/MEMS S&T Fundamentals Program (Award No: HR0011-06-1-0048).

References

Brown, M.A., Rosakis, A.J., Feng, X., Huang, Y., Ustundag, E., 2007. Thin film/substrate systems featuring arbitrary film thickness and misfit strain distributions. Part II: Experimental validation of the nonlocal stress/curvature relations. Int. J. Solids Struct. 44, 1745–1754.

Carter, J., Cowen, A., Hardy, B., Mahadevan, R., Stonefield, M., Wilcenski, S., 2005. Poly MUMPs Design Handbook. MEMSCAP Inc.. Available from: <http://www.memscap.com/en_mumps.html>.
De Groot, P., Deck, L., 1995. Surface profiling by analysis of white-light interferograms in the special frequency domain. J. Modern Opt. 42, 389–401.
Dunn, M.L., Cunningham, S.J., 2006. Thermo- and electromechanical behavior of thin-film micro and nanostructures. In: Bhushan, B. (Ed.), Chapter 56 in the Handbook of Nanotechnology, 2nd ed. Springer, Berlin.
Dunn, M.L., Zhang, Y., Bright, V.M., 2002. Deformation and structural stability of layered plate microstructures subjected to thermal loading. J. Microelectromech. Syst. 11, 372–384.
Dunn, M.L., 2007. Photomechanics of mono- and polydomain liquid crystal elastomer films. J. Appl. Phys. 102. Art. No. 013506.
Ege, E.S., Shen, Y.L., 2003. Thermomechanical response and stress analysis of copper interconnects. J. Electron. Mater. 32, 1000–1011.
Fahnline, D.E., Masters, C.B., Salamon, N.J., 1991. Thin film stress from nonspherical substrate bending measurements. J. Vac. Sci. Technol. A 9, 2483–2487.
Feng, X., Huang, Y., Rosakis, A.J., 2007a. On the stoney formula for a thin film/substrate system with nonuniform substrate thickness. J. Appl. Mech. 74, 1276–1281.
Feng, X., Huang, Y., Rosakis, A.J., 2007b. Extension of Stoney's formula to arbitrary temperature distributions in thin film/substrate systems. J. Appl. Mech. 74, 1225–1233.
Finot, M., Suresh, S., 1996. Small and large deformation of thick and thin film multilayers: effects of layer geometry, plasticity and compositional gradients. J. Mech. Phys. Solids 44, 683–721.
Finot, M., Blech, I.A., Suresh, S., Fujimoto, H., 1997. Large deformation and geometric instability of substrates with thin film deposits. J. Appl. Phys. 81, 3457–3464.
Freund, L.B., 1993. The stress distribution and curvature of a general compositionally graded semiconductor layer. J. Crystal Growth 132, 341–344.
Freund, L.B., 1996. Some elementary connections between curvature and mismatch strain in compositionally graded thin films. J. Mech. Phys. Solids 44, 723–736.
Freund, L.B., Floro, J.A., Chason, E., 1999. Extension of the Stoney formula for substrate curvature to configurations with thin substrate or large deformations. Appl. Phys. Lett. 74, 1987–1989.
Freund, L.B., 2000. Substrate curvature due to thin film mismatch strain in the nonlinear deformation range. J. Mech. Phys. Solids 48, 1159–1174.
Freund, L.B., Suresh, S., 2003. Thin Film Materials: Stress, Defect Formation and Surface Evolution. Cambridge University Press, Cambridge.
Gouldstone, A., Shen, Y.L., Suresh, S., Thompson, C.V., 1998. Evolution of stresses in passivated and unpassivated metal interconnects. J. Mater. Res. 13, 1956–1966.
Hyer, M.W., 1981. Some observations on the cured shape of thin unsymmetric laminates. J. Compos. Mater. 15, 175–194.
Hyer, M.W., 1982. The room-temperature shape of four-layer unsymmetric cross-ply laminates. J. Compos. Mater. 16, 318–340.
Keller, R.R., Geiss, R.H., Barbosa, N., Slifka, A.J., Read, D.T., 2007. Strain-induced grain growth during rapid thermal cycling of aluminum interconnects. Metall. Mater. Trans. A 38, 2263–2272.
Kim, J., Lin, L.W., 2005. Electrostatic scanning micromirrors using localized plastic deformation of silicon. J. Micromech. Microeng. 15, 1777–1785.
King, J.A., 1988. Materials Handbook for Hybrid Microelectronics. Teledyne Microelectronics, Los Angeles, California.
Masters, C.B., Salamon, N.J., 1993. Geometrically nonlinear stress-deflection relations for thin film/substrate systems. Int. J. Eng. Sci. 31, 915–925.
Masters, C.B., Salamon, N.J., 1994. Geometrically nonlinear stress-deflection relations for thin film/substrate systems with a finite element comparison. J. Appl. Mech. 61, 872–878.
Ngo, D., Huang, Y., Rosakis, A.J., Feng, X., 2006. Spatially nonuniform, isotropic misfit strain in thin films bonded on plate substrates: the relation between nonuniform film stresses and system curvatures. Thin Solid Films 515, 2220–2229.
Ngo, D., Feng, X., Huang, Y., Rosakis, A.J., Brown, M.A., 2007. Thin film/substrate systems featuring arbitrary film thickness and misfit strain distributions. Part I: Analysis for obtaining film stress from nonlocal curvature information. Int. J. Solids Struct. 44, 1745–1754.
Pajot, J., Maute, K., Zhang, Y., Dunn, M.L., 2006. Design of patterned multilayer films with eigenstrains by topology optimization. Int. J. Solids Struct. 43, 1832–1853.
Park, T.S., Suresh, S., 2000. Effects of line and passivation geometry on curvature evolution during processing and thermal cycling in copper interconnect lines. Acta Mater. 48, 3169–3175.
Park, T.S., Suresh, S., Rosakis, A.J., Ryu, J., 2003. Measurement of full-field curvature and geometrical instability of thin film-substrate systems through CGS interferometry. J. Mech. Phys. Solids 51, 2191–2211.
Sharpe, W.N., 2002. Mechanical properties of MEMS materials. In: Gad-el-Hak, M. (Ed.), A chapter in the MEMS Handbook. CRC Press, Boca Raton, FL.
Shen, Y.L., Suresh, S., Blech, I.A., 1996. Stress, curvatures, and shape changes arising from patterned lines on silicon wafers. J. Appl. Phys. 80, 1388–1398.
Shen, Y.L., 2001. Local Joule heating and overall resistance increase in void-containing aluminum interconnects. J. Electron. Mater. 30, 367–371.
Wikstrom, A., Gudmundson, P., Suresh, S., 1999a. Thermoelastic analysis of periodic thin lines deposited on a substrate. J. Mech. Phys. Solids 47, 1113–1130.
Wikstrom, A., Gudmundson, P., Suresh, S., 1999b. Analysis of average thermal stresses in passivated metal interconnects. J. Appl. Phys. 86, 6088–6095.
Wikstrom, A., Gudmundson, P., 2000. Stresses in passivated lines from curvature measurements. Acta Mater. 48, 2429–2434.
Yeo, I.S., Ho, P.S., Anderson, S.G.H., 1995a. Characterization of thermal stresses in Al(Cu) fine lines. I. Unpassivated line structures. J. Appl. Phys. 78, 945–952.
Yeo, I.S., Ho, P.S., Anderson, S.G.H., 1995b. Characterization of thermal stresses in Al(Cu) fine lines. II. Passivated line structures. J. Appl. Phys. 78, 953–961.
Zhang, Y., Dunn, M.L., 2003. Deformation of multilayer thin film microstructures during post-release cyclic thermal loading: implications for MEMS design, packaging, and reliability. J. Microelectromech. Syst. 12, 788–796.
Zhang, Y., Dunn, M.L., 2004. Geometric and material nonlinearity during the deformation of micron-scale thin-film bilayers subject to thermal loading. J. Mech. Phys. Solids 52, 2101–2126.